Biofabrication

International Society
for Biofabrication

ACCEPTED MANUSCRIPT

A 3D-printed microfluidic platform for simulating the effects of CPAP on the nasal epithelium

To cite this article before publication: Jesus Shrestha *et al* 2021 *Biofabrication* in press https://doi.org/10.1088/1758-5090/abe4c1

Manuscript version: Accepted Manuscript

Accepted Manuscript is “the version of the article accepted for publication including all changes made as a result of the peer review process, and which may also include the addition to the article by IOP Publishing of a header, an article ID, a cover sheet and/or an ‘Accepted Manuscript’ watermark, but excluding any other editing, typesetting or other changes made by IOP Publishing and/or its licensors”

This Accepted Manuscript is **© 2021 IOP Publishing Ltd**.

During the embargo period (the 12 month period from the publication of the Version of Record of this article), the Accepted Manuscript is fully protected by copyright and cannot be reused or reposted elsewhere.
As the Version of Record of this article is going to be / has been published on a subscription basis, this Accepted Manuscript is available for reuse under a CC BY-NC-ND 3.0 licence after the 12 month embargo period.

After the embargo period, everyone is permitted to use copy and redistribute this article for non-commercial purposes only, provided that they adhere to all the terms of the licence https://creativecommons.org/licences/by-nc-nd/3.0

Although reasonable endeavours have been taken to obtain all necessary permissions from third parties to include their copyrighted content within this article, their full citation and copyright line may not be present in this Accepted Manuscript version. Before using any content from this article, please refer to the Version of Record on IOPscience once published for full citation and copyright details, as permissions will likely be required. All third party content is fully copyright protected, unless specifically stated otherwise in the figure caption in the Version of Record.

View the article online for updates and enhancements.

This content was downloaded from IP address 129.78.187.10 on 03/03/2021 at 04:04

A 3D-printed Microfluidic Platform for Simulating the Effects of CPAP on the Nasal Epithelium

Jesus Shrestha[1, 2], Sean Thomas Ryan[2], Oliver Mills[2], Sareh Zhand[1], Sajad Razavi Bazaz[1], Philip Michael Hansbro[3], Maliheh Ghadiri[1, 2*], Majid Ebrahimi Warkiani[1, 4, 5*]

[1]School of Biomedical Engineering, University of Technology Sydney, Sydney, New South Wales 2007, Australia

[2]Woolcock Institute of Medical Research, Respiratory Technology Group, University of Sydney, Sydney, New South Wales 2037, Australia

[3]Centre for Inflammation, Centenary Institute & University of Technology Sydney, School of Life Sciences, Faculty of Science, Sydney, New South Wales 2050 & 2007, Australia

[4]Institute for Biomedical Materials and Devices, Faculty of Science, University of Technology Sydney, New South Wales 2007, Australia

[5]Institute of Molecular Medicine, Sechenov First Moscow State University, Moscow 119991, Russia

* Contact

Maliheh Ghadiri (maliheh.ghadiri@sydney.edu.au)

Faculty of Medicine and Health, Woolcock Institute of Medical Research, The University of Sydney, New South Wales 2037, Australia

Majid Ebrahimi Warkiani (majid.warkiani@uts.edu.au)

School of Biomedical Engineering, University Technology Sydney, Sydney, New South Wales 2007, Australia

Abstract:

Obstructive sleep apnoea (OSA) is a chronic disorder that involves a decrease or complete cessation of airflow during sleep. It occurs when the muscles supporting the soft tissues in the throat relax during sleep, causing narrowing or closure of the upper airway. Sleep apnoea is a serious medical condition with an increased risk of cardiovascular complications and impaired quality of life. Continuous positive airway pressure (CPAP) is the most effective treatment for moderate to severe cases of OSA and is effective in mild sleep apnoea. However, CPAP therapy is associated with the development of several nasal side effects and is inconvenient for the user, leading to low compliance rates. The effects of CPAP treatment on the upper respiratory system, as well as the pathogenesis of side effects, are incompletely understood and not adequately researched. To better understand the effects of CPAP treatment on the upper respiratory system, we developed an *in vitro* 3D-printed microfluidic platform. A nasal epithelial cell line, RPMI 2650, was then exposed to certain conditions to mimic the *in-vivo* environment. To create these conditions, the microfluidic device was utilized to expose nasal epithelial cells grown and differentiated at the air-liquid interface. The airflow was similar to what is experienced with CPAP, with pressure ranging between 0-20 cm of H_20. Cells exposed to pressure showed decreased barrier integrity, change in cellular shape, and increased cell death (lactate dehydrogenase release into media) compared to unstressed cells. Stressed cells also showed increased secretions of inflammatory markers IL-6 and IL-8 and had increased production of ATP. Our results suggest that stress induced by airflow leads to structural, metabolic, and inflammatory changes in the nasal epithelium, which may be responsible for developing nasal side-effects following CPAP treatment.

Keywords: *3D-printing, Microfluidics. Continuous Positive Airway Pressure, Obstructive Sleep Apnea, Nasal Epithelium, Nose-on-a-chip*

1 Introduction:

Obstructive sleep apnoea (OSA) is a common sleep disorder characterized by simultaneous instances of upper airway obstruction or collapse during sleep [1]. These obstructions cause the cessation of regular breathing and apnoea, which, when prolonged, leads to oxygen desaturation in the blood and sleep interruption resulting in non-restorative sleep [2]. The most effective treatment for OSA is positive airway pressure (PAP) devices, which function by keeping the pharyngeal pressures above a critical level and acts as a pneumatic splint to prevent airway collapse [3]. PAP systems typically consist of a flow generator delivering pressure to the respiratory tract via a tube in a facemask configuration. Continuous PAP (CPAP) is the most commonly used method of PAP and delivers constant pressure throughout both inhalation and expiration to prevent upper airway collapse.

Despite years of progress making CPAP machines smaller, more portable, quieter, and employing more comfortable masks, adherence rates continue to be unacceptably low, ranging between 30-60% [4, 5]. The majority of users report that discontinuation of use results from side effects most commonly related to the mask-skin interface, where skin breakdown, air leak, and mouth dryness are frequently reported. Nasal side effects, including epistaxis (nose-bleeds), dryness, and sinus congestion, are prevalent and substantially contribute to the high discontinuation rate [3]. During the application of the CPAP, the nasal wall and the mucosa are exposed to continuous mechanical compression, which leads to pathological responses in the cells [6-8]. Mechanical pressure may alter nasal mucociliary function, reducing respiratory defence mechanisms and adherence to treatment [9, 10]. The development of symptoms may be associated with the existing subclinical nasal inflammation and altered nasal pathology in patients with pre-existing morbidities as OSA [11-13]. Little is known about the pathogenesis of these nasal side effects, though it is speculated to be related to the induced nasal inflammation that has been reported by several studies. However, the exact mechanism is yet to be identified [10-12, 14].

To better understand the effect of pressure applied by CPAP on epithelial cells *in vitro*, air-liquid interface (ALI) cultures of the nasal epithelial cells can be used to show the effects of the airflow generated from CPAP on the cells similar to what occurs in patients. Microfluidics and organ-on-a-chip devices have recently become popular methods as they most closely replicate *in vivo* conditions [15-17]. 3D-printed prototypes of microfluidic systems are simple, cost-effective, and validated techniques with high productivity and offer versatility and reproducibility in organ-on-a-chip models [18-21]. 3D-printers allow direct printing of complete microfluidic devices and offer a wide range of printing materials [22]. Most organ-on-a-chip devices have small sample volumes and operational complexity, often requiring high-levels of training and personal skills [23]. In this study, we describe a custom 3D-printed microfluidic device based on a well-established conventional cell culture model with a user-friendly design, which is suitable for any user with minimal technical skills and microfluidic knowledge. The nasal epithelial cells cultured at the air-liquid interface (ALI) on the snapwells are exposed to PAP. This resulting cellular response with changes in inflammatory and metabolic activity, along with the barrier integrity of nasal airway monolayers, was analyzed. Defining the cellular responses may bring us closer to understanding the underlying mechanisms of the effect of positive pressure on epithelial cells and potentially to the development of improved CPAP devices with reduced side effects, thus increasing patient adherence.

2 Materials and Methods

2.1 Insert Design and Fabrication

The platform was designed to have a continuous basal media flow and controlled apical air pressure. The open-top is covered by a coverslip to ensure no air leakage (Figure 1). The device was set up inside the bio-safety cabinet and sealed with parafilm to minimize contamination. The 3D-printed platform is simple and robust, containing a central cavity to fit a 12 mm diameter snapwell polyester membrane insert (1.13 cm^2, 0.4 μm pore size, Corning Costar, USA). The central cavity has 4 access ducts, 2 for airflow, and 2 for media flow. The input air duct is connected to an external turbine, which generates airflow and pressure. This air flows over the surface of the cell monolayer on the top of the snapwell insert and exits the device through the release duct. The input media duct is connected to a syringe pump (Fusion 200, Chemyx Inc.), which generates a continuous fresh media flow beneath the snapwell membrane. This media flows out of the discharge duct and into the collection reservoir for analysis.

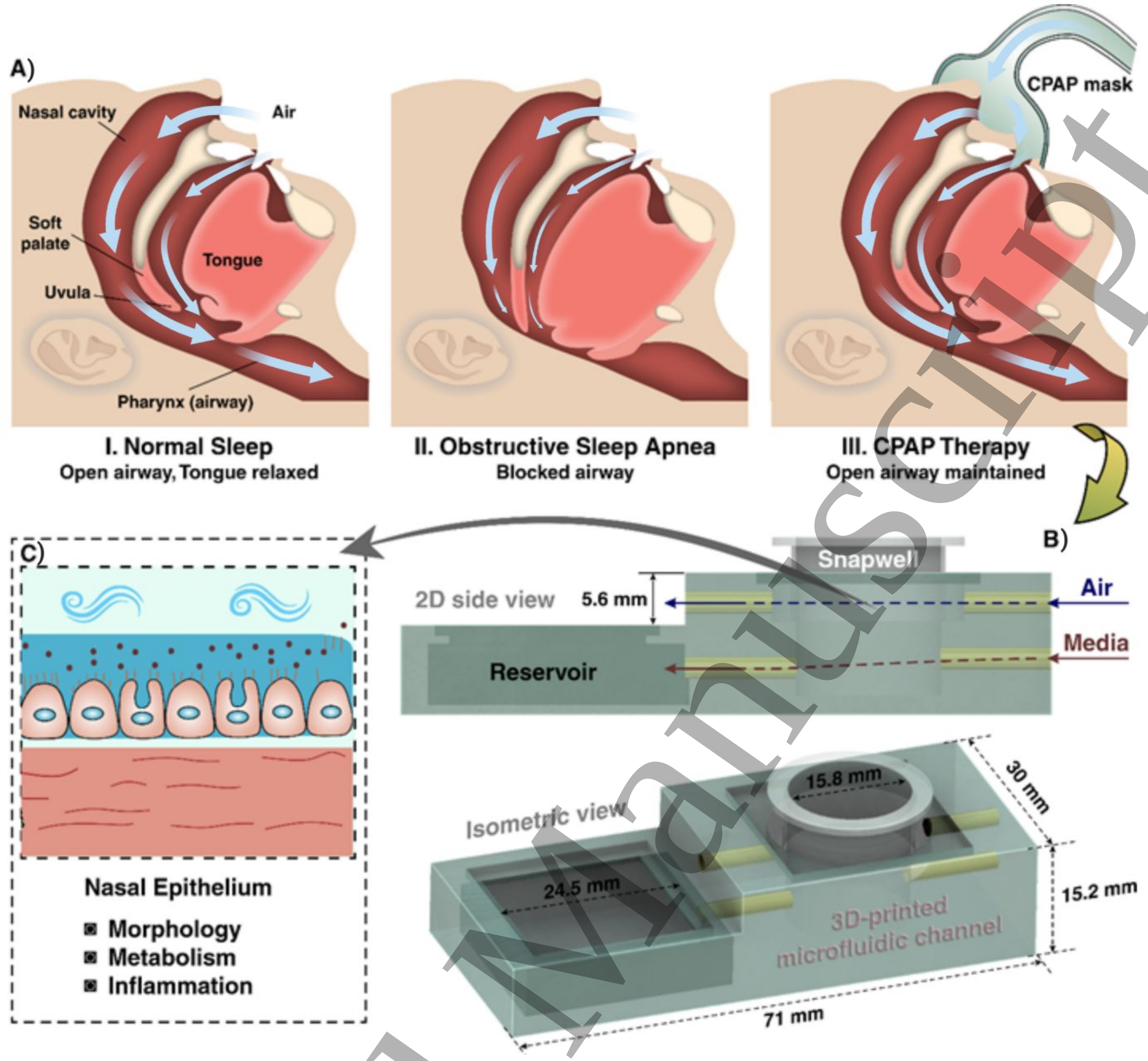

Figure 1: Use of 3D-printed microfluidic models to study the effects of CPAP on nasal epithelium: A) I. Normal open airway during sleep where airflow is continuous. **II.** The blocked airway in an OSA patient where air does not move through. **III.** Depiction of a patient receiving CPAP therapy with a steady stream of air to maintain an open airway. **B)** 2D side and isometric view of the 3D-printed model with a central cavity for a commercially available 12 mm diameter snapwell insert. Cells are cultured on the snapwell and exposed to air from the top (apical) with media flowing from the bottom (basal). A continuous flow of media is ensured in the lower channel via syringe pumps and is collected in a reservoir for analysis. **C)** Cultured nasal epithelial cells subjected to pressure ranging from 0-20 cm of H_2O from the top undergo morphological, inflammatory, and metabolic changes.

The required design was drawn in SolidWorks 2016, and then exported as an STL file format to Miicraft printer software (Utility, Version 6.1.0.t4, MiiCraft Inc). A digital light processing (DLP) 3D-printer (MiiCraft Professional 120, MiiCraft, Hsinchu, Taiwan) was used for 3D-printing the design using BV-007A resin (Creative CADworks, Toronto, Canada). After printing was complete, the printed part was carefully removed and washed thoroughly with water and Isopropyl alcohol multiple times. The part was blow-dried between each wash using a pressurized air gun to remove the resin residues and debris. Ultraviolet (UV) curing on each side of the printed part was carried out for 3 minutes. This was followed by sterilization using 100 % ethanol and UV exposure inside the biosafety cabinet for 30 minutes.

2.2 Air and Media Flow Simulation in the Channels

In order to gain insights into the behavior of air and media flow in the respective channels, the whole setup was simulated using a commercially available finite element method-based software, Comsol multiphysics 5.3a. The governing equations in this study were Navier-Stokes and continuity equations and shown in equations (1) and (2).

$$\rho(\boldsymbol{u}\cdot\nabla)\boldsymbol{u}=\nabla\cdot\left[-p\mathbf{I}+\mu\left(\nabla\boldsymbol{u}+(\nabla\boldsymbol{u})^{T}\right)\right] \tag{1}$$

$$\rho\nabla\cdot\boldsymbol{u}=0 \tag{2}$$

where, $\boldsymbol{u}$ is the velocity vector, p is pressure, ρ and μ are fluid density and dynamic viscosity, respectively. To model the air phase in the system, we developed a two-phase flow model. To track the interface of the air and liquid phases, the level-set method has been used, as shown in equation (3) [24].

$$\frac{\partial\emptyset}{\partial t}+\boldsymbol{u}\cdot\nabla\emptyset=\gamma\nabla\cdot\left(\varepsilon_{ls}\nabla\emptyset-\emptyset(1-\emptyset)\frac{\nabla\emptyset}{|\nabla\emptyset|}\right) \tag{3}$$

Here $\emptyset$ is the level set function and varies between 0 to 1. Below 0.5, elements are considered as phase 1, and greater than 0.5 elements are considered phase 2. ϵ and γ are stabilization parameters, where γ specifies the value of re-initialization of the level-set function. The maximum value of the velocity field is taken as an appropriate value for γ. ϕ ranges from 0 to 1, and the thickness of the interface is smoothly regulated by ϵ . ϵ, is selected; such it follows the same order as the minimum mesh size. The interfacial variables($\hat{n}$), the unit normal to the interface and the curvature (κ) was calculated by using equations (4) and (5), respectively.

$$\hat{n}=\frac{\nabla\emptyset}{|\nabla\emptyset|} \tag{4}$$

$$\kappa=-\nabla.\hat{n}|_{\emptyset=0.5} \tag{5}$$

The surface tension applied to the interface of two-phase fluid flow was calculated using equation (6).

$$\vec{F}_{sf} = \sigma\kappa\delta\hat{n} \tag{6}$$

σ shows the interfacial tension coefficient in [N/m]. δ is a Dirac delta function that focuses on the interface of the two phases and is calculated using equation (7).

$$\delta = 6|\nabla\emptyset||\emptyset(1 - \emptyset)| \tag{7}$$

Additionally, μ and ρ in equation (2) are smoothed by ϕ across the interface and indicated in equations (8) and (9), respectively.

$$\mu = \mu_1 + (\mu_2 - \mu_1)\emptyset \tag{8}$$

$$\rho = \rho_1 + (\rho_2 - \rho_1)\emptyset \tag{9}$$

The two-dimensional Newtonian and incompressible conditions are supposed to solve the governing equations. The inertial terms can be neglected owing to the low velocity and mass of the flows. A wetted channel wall condition with a constant contact angle is considered. γ takes the maximum value of $\vec{u}$, which is manually placed for each simulation and requires a single iteration of modelling to evaluate its value. For the media input, normal inflow velocity has been applied, whereas pressure boundary conditions with suppressed backflow has been used for the air inlet. Initial values at the upper and lower sections were considered as air and media, respectively. The boundary conditions between these two sections were considered the initial interface. The solver for the phase initialization step was set to multifrontal massively parallel sparse direct solver (MUMPS), and for the time-dependent step, a parallel sparse direct solver (PARDISO) was used.

2.3 Cell Culture

RPMI2650 cells (ATCC, IN, USA) were cultured at 2D in 75cm^2 cell culture flasks in Minimum Essential Medium (MEM) supplemented with 10% fetal bovine serum (FBS) and 1% Penicillin (Gibco, Life Technologies, Australia). The cells were placed in an incubator with a humidified atmosphere of 5 % CO_2 - 95 % O2 at 37 °C. Snapwell polyester membranes were coated with a 200 µL solution of 1 µg/mL rat collagen I in PBS (BD Biosciences, Australia) for 24 hours before cell seeding. The cells were seeded at a density of 1.5x10^5 cells/well. The medium in the apical chamber was aspirated after 24 hours to grow and differentiate at ALI. The media in the basolateral chamber was replaced every 48 hours. On day 11, snapwell membranes were fitted inside the 3D-printed platforms and connected to the OB1 Mk3 Microfluidic flow controller (Elveflow, Paris, France) and exposed to pressures of

5, 10, and 20 cm of H_2O. To maintain a dynamic state with fresh flow of media, a syringe pump (Fusion 200, Chemyx Inc.) was connected to the lower fluid channel at a flow rate of 200 µl/hr. The media was collected in a reservoir and collected for analysis. See material sources and product number in supplementary table S1.

2.4 Transepithelial electrical resistance (TEER) measurements

TEER was recorded pre- and post-experimentation to determine the integrity of the junctional connections, using an EVOM2 epithelial volt ohmmeter (World Precision Instruments, Sarasota, FL, USA). Briefly, 200 µl and 2 ml of pre-warmed PBS was added to the apical and basolateral chambers and allowed to equilibrate for 30 minutes in a cell culture incubator (humidified air with 5 % CO_2 at 37° CO_2). TEER values were calculated after subtracting the blank filters to normalize the resistance values with the snapwell inserts area (1.13 cm^2). Cells on snapwells with only media flow served as a control.

2.5 Permeation of sodium fluorescein (Flu-Na)

Barrier integrity and permeability of the RPMI2650 layer after applying positive pressure were evaluated using Flu-Na, a paracellular marker (MW 367 Da, May & Baker Ltd., Dagenham, England). After CPAP application, the snapwell was transferred to a 6 well culture plate. The apical compartment was washed with warm PBS before adding 200 µL of 2.5 mg/mL Flu-Na solution. The lower compartment was filled with 600 µL of pre-warmed PBS. Culture plates were placed in the incubator, and 200 µL samples were taken from the basal compartment at pre-determined time-points up to 3 h, replacing with fresh buffer each time to maintain sink conditions. The fluorescence readings of the Flu-Na present in the samples and standards were measured in Corning full black clear bottomed 96-well plates using a fluorescence plate reader (Infinite 200 PRO; TECAN), with excitation/emission wavelengths of 485/520 nm. Cells with no pressure applied (0 cm of H_2O pressure) were used as controls. The apparent permeability coefficient (Papp) was calculated from the linear plot of Flu-Na accumulated in the basal compartment using the following equation:

$$P_{app} = \frac{dQ}{dt.C0.A}$$

where, dQ/dt is the flux of Flu-Na across the membrane (µg/s), C_0 is the initial Flu-Na concentration (µg/ml), and A is the area of the insert membrane (cm^2).

2.6 Immunofluorescence staining

RPMI2650 cells in the inserts were washed three times with PBS and then fixed with 4% paraformaldehyde (Sigma- Aldrich, Australia) in PBS. The cell membranes were then exposed to 0.1 % (v/v) Triton X 100 (Sigma- Aldrich, Australia) with 1% (w/v) bovine serum albumin (BSA) (Sigma- Aldrich, Australia) in PBS for 60 minutes. Then the cells were incubated with 50 mM ammonium acetate in PBS for 10 minutes. The cells were then incubated with CD324 (E-cadherin) monoclonal antibody (10 µg/ml in PBS) (Invitrogen) for 1 hour at 37^0C. After further washing with PBS, AlexaFlour 594 goat anti-mouse IgG1 (10 µg/mL in PBS) (Invitrogen, Australia) was added with incubation for 1 hour at room temperature. Another washing with PBS was performed, and the cells were counterstained with 1 µg/mL 4′, 6-diamidino-2- phenylindole (DAPI) in water for 10 min. The cells on the snapwell membrane were sliced from the insert and mounted on a glass slide. The slides were coverslipped and stored at 4^0C for imaging. Cells were imaged using Nikon A1 Confocal Laser Microscope.

2.7 Effects of Positive Pressure on Inflammatory Response

The secretion of the inflammatory markers, IL-6, and IL-8, when exposed to positive pressure, was evaluated. The media collected from the reservoir of the microfluidic platform was stored at -80°C until required. Once thawed, the levels of secreted IL-6 and IL-8 in media were analyzed using IL-6 and IL-8 enzyme-linked immunosorbent assay (ELISA) kits (BD Pharmingen, U.S.A.) according to the manufacturer's instructions [25]. An Infinite 200 PRO plate reader was used to read the absorbance at 450 nm /570 nm.

2.8 Lactate Dehydrogenase (LDH) Cytotoxicity

Cellular cytotoxicity was measured through a quantitative analysis of Lactate dehydrogenase (LDH) released in the medium, using a Pierce LDH Cytotoxicity Assay Kit (ThermoScientific, U.S.A.) [26]. Then, 50 µL of the reaction mixture was prepared according to the manufacturer's protocol, and it was mixed with 50 µL of the medium collected from the microfluidic reservoir in a 96-well flat-bottom plate in triplicate wells. This was followed by incubation for 30 minutes in the dark. 50 µL of stop solution was added to each well, and absorbance was read at 490nm and 680nm using a plate reader (Infinite 200 PRO; TECAN). The percentage of cytotoxicity was calculated from the observed values. The assay is based on the chemiluminescent reaction [27], caused by the interaction of ATP with luciferase and d-luciferin;

$$\text{ATP + d-Luciferin + O2} \xrightarrow[\text{Mg}^{2+}]{\text{LUCIFERASE}} \text{Oxyluciferin + AMP + PPi + CO2 + Light}$$

2.9 Adenosine Triphosphate luminescence assay

Samples of the culture medium collected from the microfluidic reservoir were stored at -80°C until the ATP assay was performed. After thawing samples, 100 µL was added to a white opaque 96-well microplate (Perkin Elmer, U.S.A.). Then 100 µL of ATPlite 1 step reagent (Perkin Elmer, USA) was prepared following the manufacturer's instructions and was added to the well. This was followed by shaking the microplates for 2 minutes to ensure the solution was thoroughly mixed. Luminescence was then measured using the plate reader.

2.10 Statistical Analysis

Statistical testing was performed using IBM SPSS Statistics 25 software (USA). Significance was determined by one-way ANOVA, with * = $P< 0.05$ and **= $P<0.01$ considered significant. All results are expressed as means ± standard deviation (SD), and all experiments were performed at least three times.

3 Results and Discussion:

3.1 Insert Fabrication

Conventional 2D cell culture models have been used as *in vitro* models to study cell behaviors and their responses to various stimuli [28, 29]. The simplicity, efficiency, and well-established protocols of these models result in their wide use. However, these models are static and lack fluid flow, a significant physiological condition [30]. On the other hand, microfluidic systems accommodate flow conditions required for stimulating fluid mechanical forces in cells, maintaining cell-cell communication, and generating gradients of growth factors, oxygen, and other biochemical metabolites [30, 31]. The 3D-printing technique has recently gained popularity as an alternative approach to fabricate microfluidic devices [19, 32, 33]. 3D-printing allows the rapid manufacture of intricate designs with unique channels and geometries, which are unable to be matched by traditional lithography and mold techniques [34, 35]. Moreover, to simulate the effects of CPAP on the cells, an air-tight model is required, which is not obtained with gas-permeable Polydimethylsiloxane (PDMS). Thus, the integration of microfluidics and 3D-printing with well-established 2D culture models creates a dynamic *in* *vitro* experimental model, which is more physiologically relevant. A dynamic cellular environment has significant roles in regulating cellular processes, such as mucus secretion from goblet cells [36, 37]. Here we designed an air-tight multi-channel microfluidic platform suitable for a snapwell insert using a 3D printer. Snapwell inserts are well established *in vitro* culture models widely used for drug screening, migration assays, and transport studies [38]. They are easy to operate, low cost allows cell visualization throughout the experiment, and have high throughput [39].

The developed 3D-printed system permits the use of well-established conventional culture technology to culture cells separately on a permeable support to produce a confluent 3D layer of nasal epithelium that is later transferred to the microfluidic culture system. This allows cell culture at ALI and regular monitoring of the cells for differentiation, confluency and contamination. Microfluidic organ-on-a-chip models are usually designed to study specific aspects of the organ and are co-cultured with one or more cell types. In this study, a single nasal epithelial cell type was used. However, the system's design based around commercially available and well-tested snapwells, makes it easy to translate to other epithelial models like lungs, gut, liver or kidney and even expand to co-culture systems with endothelial or mesenchymal cells with few modifications [40]. The system's dynamic condition ensures a continuous supply of nutrients through media flow and the removal of metabolites, mimicking *in vivo* circulation of fluids. This system further allows the cells at ALI to be exposed to toxic compounds through air exposure route, which mimics the *in vivo* inhalation route [41]. The potential of similar systems have already been demonstrated with the study of the effects of environmental agents such as pollen extracts, diesel exhaust particles, and other nanoparticles [40, 41].

The upper half of the printed device has a circular cavity measuring 12mm in diameter with an inlet and pneumatic flow outlet. The inlet is connected to an air pressure source. The experimental setup is illustrated in Figure 2A and B. The top had an engraved square measuring for fitting a glass slip to ensure air-tightness. The lower half had a smaller circle for media to flow through, contacting, and passing nutrients to the cells growing on snapwell above. The lower circle had an inlet and outlet for media flow and an additional in-built reservoir, ensuring that the whole system was air-tight. The behaviour of air flow and media movement over time was simulated (Supplementary video 1). Based on boundary conditions applied and the atmospheric pressure set to the outlet to simulate experimental conditions (Figure 2C), air preserved its steady motion and passed through the channel. The velocity profile distribution along a line 400 μm above the air's membrane and surface velocity profile was demonstrated (Figure 2D and E) (Please check Figure S2 for the shear rate distribution in the channel). The amount of pressure applied, and the total duration of the stress on the cells is related to morphological changes, cell detachment from the membrane, and death.

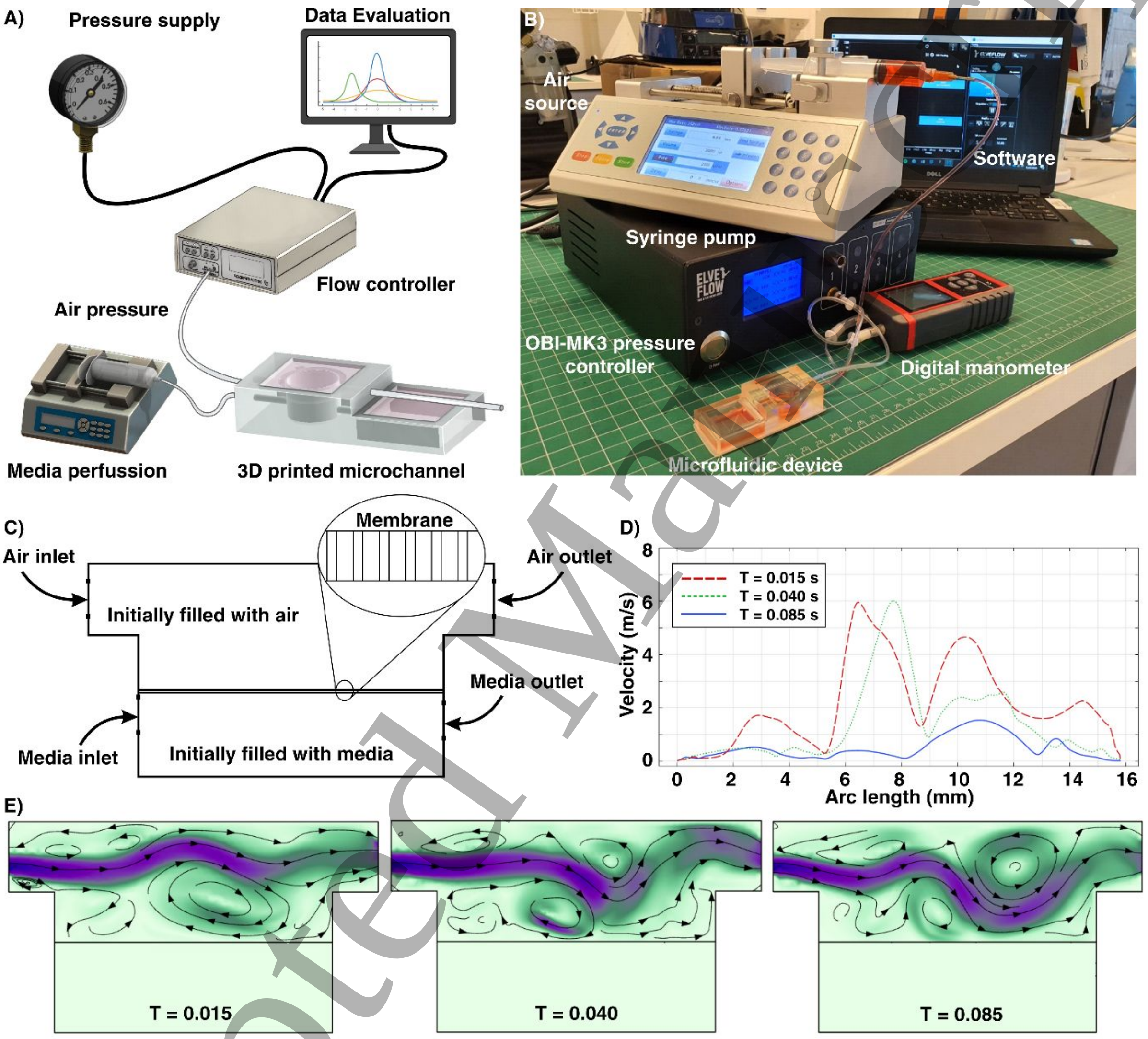

Figure 2: Experimental setup and the device: A) and B) The Elveflow OB1 MK3 pressure controller is connected to a pressure source. The pressure controller can be adjusted to range from 0-20 cm of H_2O pressure. Then it is connected to the microfluidic model with a snapwell insert. The media is injected through the lower channel using syringe pumps. After 30 minutes, the media collected in the reservoir is aspirated and preserved for further analysis. **C)** The boundary conditions of both the channels in the device for simulation. **D)** Velocity profile along the length at 400um above the membrane. **E)** Airflow with small vortices along the channel at different time points. (**D** and **E** represent 5 cm of H_2O pressure).

3.2 Biocompatibility of 3D-printed insert

With continuous research and recent advances in 3D-printing, its application has widely expanded. Rapid prototyping, low cost, and robustness make 3D-printing a favored method to fabricate microfluidic and biomedical devices [42]. However, the biocompatibility of photopolymers used in 3D-printing is a major issue that can negatively affect the resultant device for biological or biomedical applications [42-44]. 3D-printed parts may be toxic to cells or cause inflammatory responses [43]. Moreover, the 3D-printing technique and the parts may not be sterile, which increases the likelihood of media contamination. To test our 3D-printer resin's biocompatibility, BV007, a part measuring 4 cm X 2 cm, was printed and thoroughly washed with IPA and 100% ethanol. The part was then exposed to UV-light for 30 minutes before dipping in 6 well plates filled with culture media and incubated for 48 hours. RPMI2650 cells were then cultured in different 6 well plates with the collected media. The viability of the cells was checked using live dead staining over 5 days (Figure 3A and B). The cells remained alive and grew well, demonstrating the resin used in our 3D-printed inserts was suitable for cell culture. Moreover, we compared the growth progress of the cells in media with and without the 3D-printed resin sample. Cells were seeded in different 6 well plates with a seeding density of 300,000 cells per well. In one plate, the media dipped with the 3D-printed resin part was used, whereas conventional media was used in the other. The 3D-printed resin part was washed multiple times with 100% ethanol, followed by UV treatment for 30 minutes, to sterilize it and minimize contamination and toxicity [42]. The morphology and growth of the cells were observed under an Olympus Ix73 Inverted Microscope. After trypsinization, the cells were counted with a trypan blue staining procedure using a haemocytometer [45]. The average cell number of three wells were calculated and plotted. Figure 3C shows the cell growth curve of the RPMI2650 cells over time. Cells grown in media with and without the 3D-printed part demonstrated comparable cell-growth.

ELISA was performed to test for any effects of the cured resin on the secretion of the inflammatory markers from the cultured cells. There was no significant difference in the secretion of IL-6 and IL-8 from RPMI 2650 cells cultured in media with and without 3D-printed resin (Figure 3D). Since the pressure application duration was only 30 minutes, the cells were exposed to the 3D-printed microfluidic device resin for only a short duration. Thus, the resin BV007 was used for printing the inserts and in all of our subsequent experiments. The cells were only exposed to air pressure for 30 minutes in this study. The long-term culture of the cell monolayer in the device was not evaluated in the system as long term exposure of cells grown at ALI leads to the drying of the epithelial surface, which leads to cellular stress and cell death. However, during the optimization, cells were cultured in the device for 48 hours to test for any cracks, culture media leakage, and media collection in the reservoir. No visible cracks on the device or leakage of media were observed and the waste media was collected in the reservoir. However, long-term exposure to media can lead to leaching of the resin with biological consequences. The curing protocols will require optimization and the effects evaluated accordingly, even changing the type of the resin used for long-term exposures.

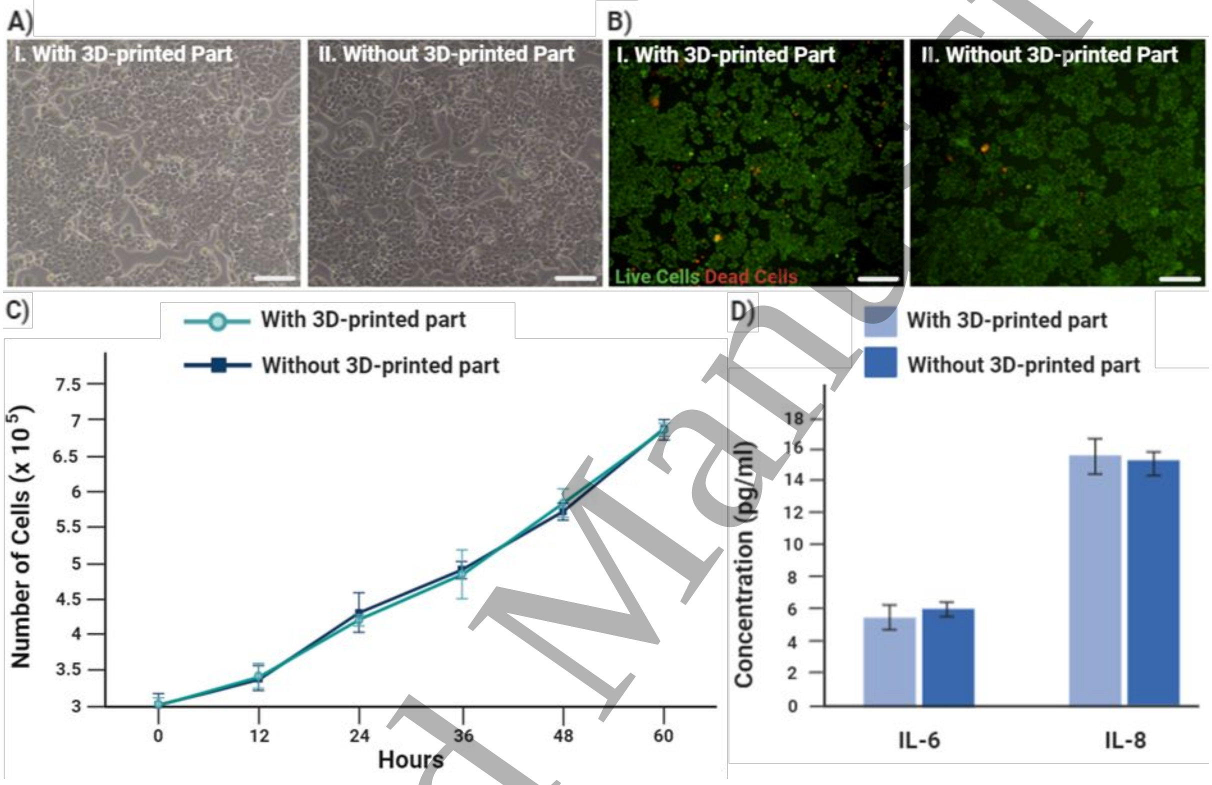

Figure 3: Biocompatibility of the 3D-printed part: A) I. and II. Microscopic images of RPMI2650 cells cultured in 6 well plates for 48 hrs using culture medium with and without immersed 3D-printed part (Scale: 50 µm) **B) I. and II.** live and dead imaging of the cells (Scale: 100 µm). **C)** Comparison of the growth curves of cells cultured in well plates using culture medium with and without exposure to the 3D-printed part. **D)** Comparison of the secretion of the pro-inflammatory markers IL-6 and IL-8 concentrations from cultured cells in media with or without exposure to 3D-printed resin.

3.3 Barrier Integrity

Epithelial cells are connected to each other via intercellular junctions that are required for cell function [46]. Tight junctions serve as a barrier and regulate cellular diffusion and transport processes [47]. Barrier integrity, which is a function of tight junctions, is vital for maintaining homeostasis and the physiology of the tissue. TEER is the measurement of electrical resistance across an epithelial or endothelial monolayer [46]. It is a non-invasive, highly sensitive, and reliable quantitative technique to verify the permeability of the epithelium layer and its barrier integrity. The ability to be employed in real-time with no damage to cells makes TEER a widely used method for monitoring cells in different stages of growth and differentiation [46]. TEER measurements were performed before and after experimentation to determine the effects of a range of pressures on barrier integrity of RPMI2650 monolayers. Before the experiment, TEER values ranged between 90-130 Ω cm^2, which is similar to those reported for that same cell line [48, 49]. However, the barrier integrity of the cell monolayer decreased with increasing pressure, indicated by decreases in TEER values (Figure 4A). The application of pressure had dose-dependent effects and was maximal at 20 compared to 5 and 10 cm of H_20. These results are different from studies using the same cell-lines, most probably due to the duration of pressure application, where pressure was applied for over 8 hours [50]. To further evaluate the effects of pressure on cell connections, staining of a tight junction protein, E-cadherin, was performed. E-cadherin levels were inversely proportional to pressure, with minimal levels occurring at 20 cm of H_20 pressure and gradually increasing with a decrease in pressure (Figure 4B).

To support the findings of TEER measurements and expression of E-cadherin with different pressure application, permeation studies of Flu-Na were performed. The transport of Flu-Na across the cell layers was performed after applying 5, 10, and 20 cm of H_20 pressure for 30 minutes and compared to controls with no pressure applied. In agreement with the morphological and electrophysiological results, Flu-Na transport across the cell layer was significantly increased showing apparent permeability after applying pressure (Figure 4C). The cell layer was more permeable to the paracellular marker with decreased P_{app} values after 30 minutes of pressure application compared to controls. This indicates that higher pressures result in the disruption of cellular tight junctions, thus reducing epithelial monolayer barrier integrity in 3D cultures.

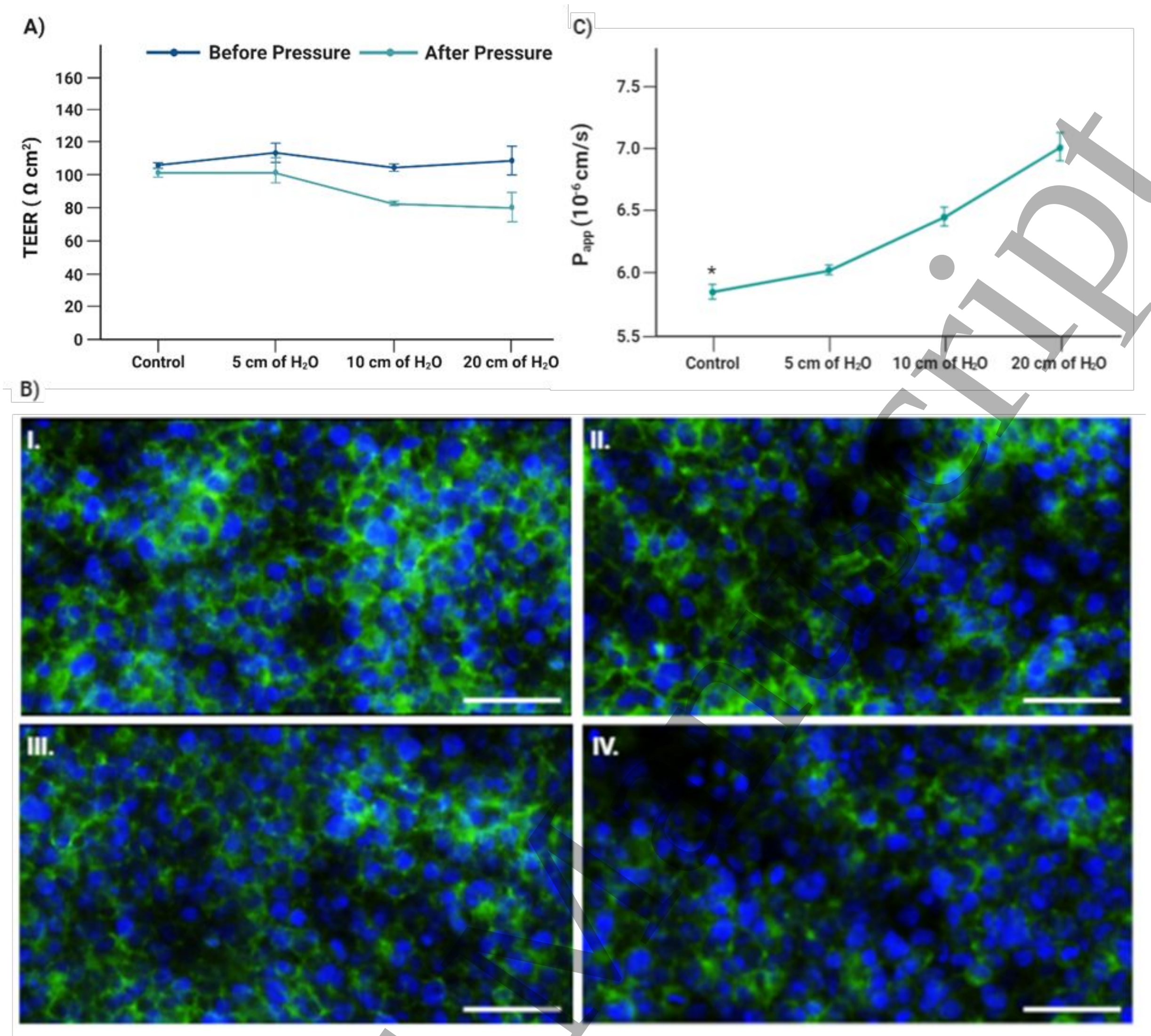

Figure 4: Barrier integrity of the RPMI2650 cell monolayer: A) TEER values (Ω cm^2) of RPMI2650 on snapwells before and after the application of stress at 0, 5, 10, and 20 cm of H_20 pressure. **B) I-IV.** Confocal microscope images of the tight junction protein, E-cadherin (green), nuclei (blue), after applying stress at 0, 5, 10, and 20 cm of H_20 pressure, respectively. Scale: 100 µm. **C)** Apparent permeability coefficient (Papp) of cell layers at control (0 cm H_20), 5, 10, and 20 cm H_2O.

3.4 Changes in the Nasal Inflammation

Despite the advantages of the CPAP, it is usually associated with a high occurrence of developing side effects and, ultimately, non-compliance [51]. The development of nasal symptoms is often linked to the induction of local inflammation, with numerous studies reporting the local and systemic inflammatory changes with CPAP [12, 52-54]. It is likely the mechanical stimulus caused by compression of the nasal walls from CPAP that triggers inflammation [55]. However, the effects of CPAP on local and systemic inflammation remain controversial, and several studies have reported the suppression of inflammation and oxidative stress levels in OSA patients [14, 55, 56]. In this study, the cytokine concentration released by the cultured RPMI2650 cells on exposure to CPAP pressure was measured. CPAP was associated with the pressure-dependent release of both IL-6 and IL-8 (Figure 5A and B). The release of IL-6, a critical pro-inflammatory cytokine, and IL-8, a neutrophil chemotactic factor to inflammation site, were induced by 20 cm of H_2O pressure. Most patients with OSA have increased levels of pro-inflammatory cytokines and systemic inflammatory markers. Most studies focusing on inflammatory responses induced by CPAP have been limited to OSA patients and show associations with inflammation and several metabolic aberrations. Thus, the study of the effects of CPAP on normal nasal airway epithelium provides insight into the normal physiology and inflammatory response to the range of pressure applied during CPAP treatment.

3.5 Changes in Metabolic Activities

All cells experience and respond to a variety of mechanical stimuli, both intracellular and extracellular [57, 58]. Cells respond by altering their division rate, differentiation, secretions, ion transport, gene expression, exocytosis, and endocytosis [58-60]. Moreover, exposure to mechanical pressure stimulates the secretion of extracellular matrix proteins, growth factors, enzymes, hormones, adenosine triphosphate (ATP), nitric oxide (NO), and other signalling molecules [58]. ATP is the main intracellular energy currency synthesized in mitochondria [61]. Also, it is present in all metabolically active cells and links catabolic and anabolic processes [27]. Conditions of acute stress, such as cell injury, early stages of apoptosis activation, or oxidative stress, have shown to induce mitochondrial elongation, resulting in increased ATP synthesis [62-64]. To measure the effects of CPAP pressure on ATP, an ATP-based luminescence kit, the ATPlite 1step assay system was used. Cells stimulated with 20 cm of H_2O pressure had increased levels of intracellular ATP, which was significantly higher compared to cells exposed to 5, 10 cm of H_2O pressure and controls (Figure 5C). Increased ATP production can be associated with increased activity of mitochondria. Mitochondria are important cell stress sensors that communicate with the rest of the cell to stimulate cellular processes [65, 66]. When cells are stimulated by pressure, they raise their metabolic activity with increased mitochondrial activity and greater ATP production.

An LDH cytotoxicity assay was performed to analyze the effects of pressure on cell membrane integrity. Cytotoxicity testing is a commonly measured biological parameter conducted after experimental manipulation to assess the health of cells [67]. When interacting with mechanical stimuli, toxins, or stressors, mammalian cells undergo structural and morphological changes resulting in changes to plasma membrane tension and loss of membrane integrity [68]. This promotes the leakage of cell contents into the culture medium [58, 69]. Thus, cytotoxicity assays to measure cell membrane integrity can be quantified by measuring the intracellular enzyme markers in the extracellular environment [67]. LDH is a cytosolic enzyme present in cells that are released into culture media if the plasma membrane has been damaged [70]. The LDH activity of cells under 20 cm of H_2O pressure was significantly higher compared to 5, 10 cm of H_2O pressure, and controls in a dose-dependent fashion (Figure 5D). The viability of the cells in the inserts after application of the pressures 5, 10, and 20 cm of H_2O was also assessed by using Trypan blue staining (results are shown in the supplementary information, Figure S1).

In summary, 20 cm of H_2O pressure has significant effects on metabolic activity and membrane integrity of cells, as increased pressure is associated with ATP production and LDH release.

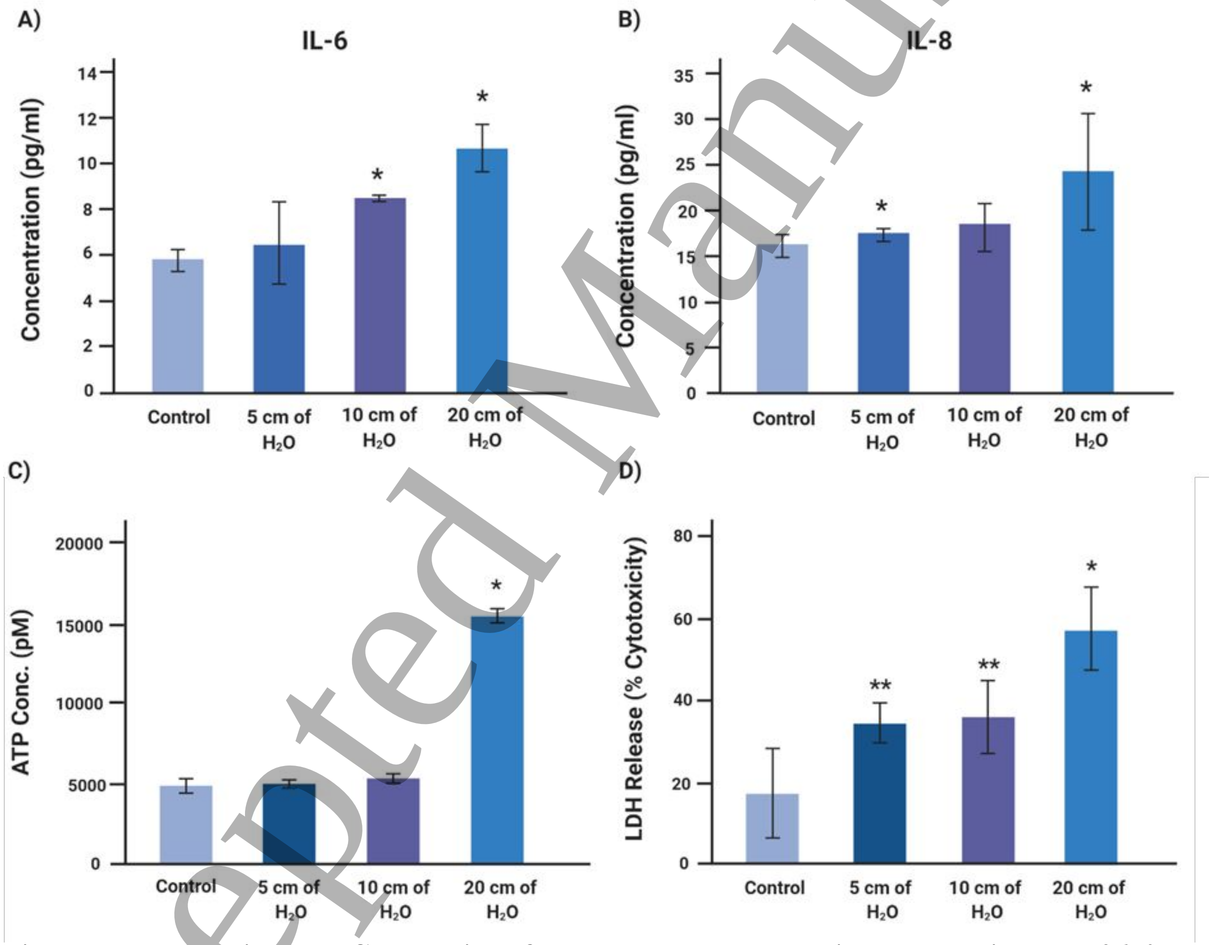

Figure 5: Pressure-induced Changes in Inflammatory and Metabolic responses in RPMI2650 cell monolayers: A) and B) Pro-inflammatory marker IL-6 and IL-8 concentrations at baseline (0 cm of H_2O) and with exposure to continuous positive pressures of 5, 10, and 20 cm of H_2O for 30 minutes. **C)** Bioluminescence assay showing ATP production at baseline and with continuous positive pressure of 5, 10, and 20 cm of H_2O for 30 minutes. **D)** Lactate dehydrogenase (LDH) release assay. There were significant increases in the release of LDH from cells with pressure increases that were maximal at 20 cm of H_2O. Data are presented as mean±SD, n=3. *: $p<0.05$, **: $p<0.01$.

Conclusion:

Here, we present a robust and easily operatable model developed with the synergism of progressive technologies in 3D-printing and microfluidics, with a well-established *in vitro* culture model to study the physiological changes occurring in nasal epithelial cells subjected to airflow induced pressure/stress to mimic the effects of CPAP. Cells cultured at ALI were exposed to airflow-induced stress ranging from 0-20 cm of H_2O for 30 minutes. The barrier integrity of the epithelial monolayer decreased when subjected to pressure in a dose-dependent fashion that was maximal at 20 cm of H_20 compared to unstressed cells. Immunostaining of a tight junction protein, E-cadherin, showed reduced levels in stressed cells. Media was analyzed for the inflammatory markers IL-6 and IL-8, both of which were significantly increased in stressed cells. Moreover, increased release of LDH and ATP into the media from the cells was observed in the stressed cells. Our system does not completely reproduce the exact physiological and structural changes occurring in the human nasal airway during CPAP therapy, but it provides powerful insights into the effect that dynamic pressure has on epithelial cells. Our results suggest that stress-induced by airflow during CPAP leads to structural, metabolic, and inflammatory changes on the nasal epithelium. This may be responsible for the development of nasal side-effects following CPAP, leading to poor patient compliance. With further progress through the addition of features relevant to specific studies, co-culture of different cell types, or the use of primary cells, advanced *in vitro* models have the potential to positively impact a wide array of research fields.

Declaration of Competing Interest

The authors declare no competing financial interests.

Acknowledgments

This work was supported by the Australian Research Council through Discovery Project Grants (Grant Nos. DP170103704 and DP180103003) and the National Health and Medical Research Council (NHMRC) through the Career Development Fellowship (Grant No. APP1143377). Prof Hansbro is a recipient of an NHMRC Investigator Grant (1175134). Dr. Ghadiri is the recipient of the Ann Woolcock Fellowship from Woolcock Institute of Medical Research.

Supporting Information

Supplementary data for this article can be found online at:

ORCID iDs

Jesus Shrestha https://orcid.org/0000-0003-3692-6676

Sajad Razavi Bazaz https://orcid.org/0000-0002-6419-3361

Philip M. Hansbro https://orcid.org/0000-0002-4741-3035

Maliheh Ghadiri https://orcid.org/0000-0002-7371-9505

References:

1. Senaratna, C.V., et al., *Prevalence of obstructive sleep apnea in the general population: a systematic review.* Sleep medicine reviews, 2017. **34**: p. 70-81.
2. Punjabi, N.M., *The epidemiology of adult obstructive sleep apnea.* Proceedings of the American Thoracic Society, 2008. **5**(2): p. 136-143.
3. Gharibeh, T. and R. Mehra, *Obstructive sleep apnea syndrome: natural history, diagnosis, and emerging treatment options.* Nature and science of sleep, 2010. **2**: p. 233.
4. Weaver, T.E. and A.M. Sawyer, *Adherence to continuous positive airway pressure treatment for obstructive sleep apnea: implications for future interventions.* The Indian journal of medical research, 2010. **131**: p. 245.
5. Weaver, T.E. and R.R. Grunstein, *Adherence to continuous positive airway pressure therapy: the challenge to effective treatment.* Proceedings of the American Thoracic Society, 2008. **5**(2): p. 173-178.
6. Kobayashi, S., et al., *Effect of mechanical compression on the lumbar nerve root: localization and changes of intraradicular inflammatory cytokines, nitric oxide, and cyclooxygenase.* Spine, 2005. **30**(15): p. 1699-1705.
7. Tschumperlin, D.J. and J.M. Drazen, *Chronic effects of mechanical force on airways.* Annu. Rev. Physiol., 2006. **68**: p. 563-583.
8. Devouassoux, G., et al., *Sleep apnea is associated with bronchial inflammation and continuous positive airway pressure–induced airway hyperresponsiveness.* Journal of Allergy and Clinical Immunology, 2007. **119**(3): p. 597-603.
9. Lorenzi, G., et al., *Correlation between rheologic properties and in vitro ciliary transport of rat nasal mucus.* Biorheology, 1992. **29**(4): p. 433-440.
10. Saka, C., et al., *The effects of CPAP treatment on nasal mucosa in patients with obstructive sleep apnea.* European Archives of Oto-Rhino-Laryngology, 2012. **269**(9): p. 2065-2067.
11. Gelardi, M., et al., *Regular CPAP utilization reduces nasal inflammation assessed by nasal cytology in obstructive sleep apnea syndrome.* Sleep Medicine, 2012. **13**(7): p. 859-863.
12. AlAhmari, M.D., et al., *Dose response of continuous positive airway pressure on nasal symptoms, obstruction and inflammation in vivo and in vitro.* European Respiratory Journal, 2012. **40**(5): p. 1180-1190.

13. Shadan, F.F., et al., *Nasal cytology: a marker of clinically silent inflammation in patients with obstructive sleep apnea and a predictor of noncompliance with nasal CPAP therapy.* Journal of Clinical Sleep Medicine, 2005. **1**(03): p. 266-270.
14. Xie, X., et al., *Effects of continuous positive airway pressure therapy on systemic inflammation in obstructive sleep apnea: a meta-analysis.* Sleep medicine, 2013. **14**(11): p. 1139-1150.
15. Shrestha, J., et al., *Lung-on-a-chip: the future of respiratory disease models and pharmacological studies.* Critical Reviews in Biotechnology, 2020. **40**(2): p. 213-230.
16. Huh, D., G.A. Hamilton, and D.E. Ingber, *From 3D cell culture to organs-on-chips.* Trends in Cell Biology, 2011. **21**(12): p. 745-754.
17. Bhatia, S.N. and D.E. Ingber, *Microfluidic organs-on-chips.* Nat Biotechnol, 2014. **32**(8): p. 760-72.
18. Bazaz, S.R., et al., *3D Printing of Inertial Microfluidic Devices.* Scientific reports, 2020. **10**(1): p. 1-14.
19. Ho, C.M.B., et al., *3D printed microfluidics for biological applications.* Lab on a Chip, 2015. **15**(18): p. 3627-3637.
20. Yi, H.-G., H. Lee, and D.-W. Cho, *3D printing of organs-on-chips.* Bioengineering, 2017. **4**(1): p. 10.
21. Syed, M.S., et al., *Particle movement and fluid behavior visualization using an optically transparent 3D-printed micro-hydrocyclone.* Biomicrofluidics, 2020. **14**(6): p. 064106.
22. Brennan, M.D., M.L. Rexius-Hall, and D.T. Eddington, *A 3D-printed oxygen control insert for a 24-well plate.* PLoS One, 2015. **10**(9): p. e0137631.
23. Campana, O. and D. Wlodkowic, *Ecotoxicology goes on a chip: embracing miniaturized bioanalysis in aquatic risk assessment.* Environmental science & technology, 2018. **52**(3): p. 932-946.
24. Mollajan, M., S.R. Bazaz, and A.A. Mehrizi, *A Thoroughgoing Design of a Rapid-cycle Microfluidic Droplet-based PCR Device to Amplify Rare DNA Strands.* Journal of Applied Fluid Mechanics, 2018. **11**(1): p. 21-29.
25. Hansbro, P.M., et al., *Importance of mast cell Prss31/transmembrane tryptase/tryptase-γ in lung function and experimental chronic obstructive pulmonary disease and colitis.* Journal of Biological Chemistry, 2014. **289**(26): p. 18214-18227.
26. Gold, M., et al., *Mucosal production of uric acid by airway epithelial cells contributes to particulate matter-induced allergic sensitization.* Mucosal Immunology, 2016. **9**(3): p. 809-820.
27. Crouch, S., et al., *The use of ATP bioluminescence as a measure of cell proliferation and cytotoxicity.* Journal of immunological methods, 1993. **160**(1): p. 81-88.
28. Duval, K., et al., *Modeling Physiological Events in 2D vs. 3D Cell Culture.* Physiology, 2017. **32**(4): p. 266-277.
29. Hsu, A.C., et al., *Critical role of constitutive type I interferon response in bronchial epithelial cell to influenza infection.* PloS one, 2012. **7**(3): p. e32947.
30. Inamdar, N.K. and J.T. Borenstein, *Microfluidic cell culture models for tissue engineering.* Current Opinion in Biotechnology, 2011. **22**(5): p. 681-689.
31. Meyvantsson, I. and D.J. Beebe, *Cell culture models in microfluidic systems.* Annu. Rev. Anal. Chem., 2008. **1**: p. 423-449.
32. Waldbaur, A., et al., *Let there be chip—towards rapid prototyping of microfluidic devices: one-step manufacturing processes.* Analytical Methods, 2011. **3**(12): p. 2681-2716.
33. Vasilescu, S.A., et al., *3D printing enables the rapid prototyping of modular microfluidic devices for particle conjugation.* Applied Materials Today, 2020. **20**: p. 100726.

34. Shrestha, J., et al., *A Rapidly Prototyped Lung-on-a-chip Model Using 3D-Printed Molds.* Organs-on-a-Chip, 2020: p. 100001.
35. Razavi Bazaz, S., et al., *3D Printing of Inertial Microfluidic Devices.* Scientific Reports, 2020. **10**(1): p. 5929.
36. Even-Tzur, N., et al., *Mucus secretion and cytoskeletal modifications in cultured nasal epithelial cells exposed to wall shear stresses.* Biophysical journal, 2008. **95**(6): p. 2998-3008.
37. Reid, A.T., et al., *Blocking Notch3 signaling abolishes MUC5AC production in airway epithelial cells from individuals with asthma.* American Journal of Respiratory Cell and Molecular Biology, 2020. **62**(4): p. 513-523.
38. Katt, M.E., et al., *In vitro tumor models: advantages, disadvantages, variables, and selecting the right platform.* Frontiers in bioengineering and biotechnology, 2016. **4**: p. 12.
39. Stone, N.L., T.J. England, and S.E. O'Sullivan, *A novel transwell blood brain barrier model using primary human cells.* Frontiers in cellular neuroscience, 2019. **13**: p. 230.
40. Blume, C., et al., *Temporal monitoring of differentiated human airway epithelial cells using microfluidics.* PLoS One, 2015. **10**(10): p. e0139872.
41. Hiemstra, P.S., et al., *Human lung epithelial cell cultures for analysis of inhaled toxicants: Lessons learned and future directions.* Toxicology in vitro, 2018. **47**: p. 137-146.
42. Oskui, S.M., et al., *Assessing and reducing the toxicity of 3D-printed parts.* Environmental Science & Technology Letters, 2016. **3**(1): p. 1-6.
43. Alifui-Segbaya, F., et al., *Biocompatibility of photopolymers in 3D printing.* 3D Printing and Additive Manufacturing, 2017. **4**(4): p. 185-191.
44. Zhu, F., et al., *Assessment of the biocompatibility of three-dimensional-printed polymers using multispecies toxicity tests.* Biomicrofluidics, 2015. **9**(6): p. 061103.
45. Beckett, E.L., et al., *TLR2, but not TLR4, is required for effective host defence against Chlamydia respiratory tract infection in early life.* PloS one, 2012. **7**(6): p. e39460.
46. Srinivasan, B., et al., *TEER measurement techniques for in vitro barrier model systems.* Journal of laboratory automation, 2015. **20**(2): p. 107-126.
47. Matter, K. and M.S. Balda, *Functional analysis of tight junctions.* Methods, 2003. **30**(3): p. 228-234.
48. Wengst, A. and S. Reichl, *RPMI 2650 epithelial model and three-dimensional reconstructed human nasal mucosa as in vitro models for nasal permeation studies.* European journal of pharmaceutics and biopharmaceutics, 2010. **74**(2): p. 290-297.
49. Pozzoli, M., et al., *Application of RPMI 2650 nasal cell model to a 3D printed apparatus for the testing of drug deposition and permeation of nasal products.* European Journal of Pharmaceutics and Biopharmaceutics, 2016. **107**: p. 223-233.
50. Grau-Bartual, S., et al., *Effect of continuous positive airway pressure treatment on permeability, inflammation and mucus production of human epithelial cells.* ERJ Open Research, 2020. **6**(2).
51. Pépin, J.L., et al., *Side effects of nasal continuous positive airway pressure in sleep apnea syndrome: study of 193 patients in two French sleep centers.* Chest, 1995. **107**(2): p. 375-381.
52. Koutsourelakis, I., et al., *Nasal inflammation in sleep apnoea patients using CPAP and effect of heated humidification.* European Respiratory Journal, 2011. **37**(3): p. 587-594.
53. Almendros, I., et al., *Continuous positive airway pressure (CPAP) induces early nasal inflammation.* Sleep, 2008. **31**(1): p. 127-131.

54. Skoczynski, S., et al., *Short-term CPAP treatment induces a mild increase in inflammatory cells in patients with sleep apnoea syndrome.* Rhinology, 2008. **46**(2): p. 144.

55. Karamanlı, H., et al., *Influence of CPAP treatment on airway and systemic inflammation in OSAS patients.* Sleep and Breathing, 2014. **18**(2): p. 251-256.

56. Baessler, A., et al., *Treatment for sleep apnea by continuous positive airway pressure improves levels of inflammatory markers-a meta-analysis.* Journal of inflammation, 2013. **10**(1): p. 13.

57. Hamill, O.P. and B. Martinac, *Molecular basis of mechanotransduction in living cells.* Physiological reviews, 2001. **81**(2): p. 685-740.

58. Apodaca, G., *Modulation of membrane traffic by mechanical stimuli.* American Journal of Physiology-Renal Physiology, 2002. **282**(2): p. F179-F190.

59. Dai, J. and M. Sheetz. *Regulation of endocytosis, exocytosis, and shape by membrane tension*. in *Cold Spring Harbor symposia on quantitative biology*. 1995. Cold Spring Harbor Laboratory Press.

60. Edwards, Y.S., *Stretch stimulation: its effects on alveolar type II cell function in the lung.* Comparative Biochemistry and Physiology Part A: Molecular & Integrative Physiology, 2001. **129**(1): p. 245-260.

61. Fuhrman, B.P. and J.J. Zimmerman, *Pediatric Critical Care E-Book*. 2016: Elsevier Health Sciences.

62. Liesa, M. and O.S. Shirihai, *Mitochondrial dynamics in the regulation of nutrient utilization and energy expenditure.* Cell metabolism, 2013. **17**(4): p. 491-506.

63. Tondera, D., et al., *SLP-2 is required for stress-induced mitochondrial hyperfusion.* The EMBO journal, 2009. **28**(11): p. 1589-1600.

64. Dua, K., et al., *Increasing complexity and interactions of oxidative stress in chronic respiratory diseases: An emerging need for novel drug delivery systems.* Chemico-Biological Interactions, 2019. **299**: p. 168-178.

65. Delon, L.C., et al., *A systematic investigation of the effect of the fluid shear stress on Caco-2 cells towards the optimization of epithelial organ-on-chip models.* Biomaterials, 2019. **225**: p. 119521.

66. Barbour, J.A. and N. Turner, *Mitochondrial stress signaling promotes cellular adaptations.* International journal of cell biology, 2014. **2014**.

67. Cho, M.-H., et al., *A bioluminescent cytotoxicity assay for assessment of membrane integrity using a proteolytic biomarker.* Toxicology in vitro, 2008. **22**(4): p. 1099-1106.

68. Leist, M. and M. Jäättelä, *Four deaths and a funeral: from caspases to alternative mechanisms.* Nature reviews Molecular cell biology, 2001. **2**(8): p. 589-598.

69. Riss, T.L. and R.A. Moravec, *Use of multiple assay endpoints to investigate the effects of incubation time, dose of toxin, and plating density in cell-based cytotoxicity assays.* Assay and drug development technologies, 2004. **2**(1): p. 51-62.

70. Korzeniewski, C. and D.M. Callewaert, *An enzyme-release assay for natural cytotoxicity.* Journal of immunological methods, 1983. **64**(3): p. 313-320.